Photoelectrochemical reaction and H2 generation at zero bias optimized by carrier concentration of n-type GaN

doi: 10.1063/1.2432116

Photoelectrochemical reaction and H_2 generation at zero bias optimized by carrier concentration of *n*-type GaN

Masato Ono
Department of Applied Physics, Tokyo University of Science, 1-3 Kagurazaka, Shinjyuku, Tokyo 162-8601, Japan

Katsushi Fujii
Nakamura Inhomogeneous Crystal Project, Exploratory Research for Advanced Technology, Japan Science and Technology Agency, Tokyo University of Science, 1-3 Kagurazaka, Shinjyuku, Tokyo 162-8601, Japan and Center for Interdisciplinary Research, Tohoku University, Aramaki aza Aoba 6-3, Aoba-ku, Sendai 980-8578, Japan

Takashi Ito and Yasuhiro Iwaki
Department of Applied Physics, Tokyo University of Science, 1-3 Kagurazaka, Shinjyuku, Tokyo 162-8601, Japan

Akira Hirako
Nakamura Inhomogeneous Crystal Project, Exploratory Research for Advanced Technology, Japan Science and Technology Agency, Tokyo University of Science, 1-3 Kagurazaka, Shinjyuku, Tokyo 162-8601, Japan

Takafumi Yao
Center for Interdisciplinary Research, Tohoku University, Aramaki aza Aoba 6-3, Aoba-ku, Sendai 980-8578, Japan and Institute of Materials Research, Tohoku University, 2-1-1 Katahira, Aoba-ku, Sendai 980-8577, Japan

Kazuhiro Ohkawa
Department of Applied Physics, Tokyo University of Science, 1-3 Kagurazaka, Shinjyuku, Tokyo 162-8601, Japan and Nakamura Inhomogeneous Crystal Project, Exploratory Research for Advanced Technology, Japan Science and Technology Agency, Tokyo University of Science, 1-3 Kagurazaka, Shinjyuku, Tokyo 162-8601, Japan

(Received 11 April 2006; accepted 12 December 2006; published online 6 February 2007)

The authors studied the photoelectrochemical properties dependent on carrier concentration of *n*-type GaN. The photocurrent at zero bias became the maximum value at the carrier concentration of 1.7×10^{17} cm^{-3}. Using the sample optimized carrier concentration, the authors achieved H_2 gas generation at a Pt counterelectrode without extra bias for the first time. The authors also discussed the mechanism of the dependence of photocurrent on the carrier concentration of GaN. © *2007 American Institute of Physics*. [DOI: 10.1063/1.2432116]

I. INTRODUCTION

Direct photoelectrolysis by solar power is a promising method to produce H_2 gas from water.[1] When one splits water in a photoelectrochemical cell using semiconductor, the band-edge energy positions of semiconductor are very important. Those of many III–V and II–VI semiconductors are suitable for photoelectrolysis,[2] however, the semiconductors are oxidized and corroded easily. The band-edge energy positions of GaN have been shown to be enough to split water.[3–6] GaN shows considerable resistance to corrode in many aqueous solutions in the dark. Thus, the photoelectrochemical properties, especially the water splitting, of nitride semiconductors have been investigated. We also reported H_2 gas generation at a counterelectrode by H^+-ion reduction using a GaN or InGaN photoelectrode with small amount of bias.[5,7] On the other hand, the oxidation at the *n*-type GaN surface by photoelectrolysis as pointed out to be simultaneous oxygen generation and GaN photocorrosion.[5] This GaN corrosion was reported to suppress in the presence of Cl^- ions because Cl^--ion oxidation was easy to occur.[8]

Photoelectrochemical properties of GaN were not well investigated besides the photocorrosion problem. Especially, the effects of the electrical properties of GaN were not reported. Furthermore, H_2 gas generation at a counterelectrode using a *n*-type GaN photoelectrode with zero bias was not observed because of the small photocurrent.

In this paper, we report the photoelectrochemical properties dependent on the carrier concentration of *n*-type GaN and propose a simple model to explain this dependence. H_2 gas generation at zero bias using the GaN optimized carrier concentration is also reported.

II. EXPERIMENT

Working electrodes were Si-doped *n*-type GaN layers on (0001) sapphire substrates with low-temperature GaN buffer layers grown by atmospheric-pressure metal organic vapor-phase epitaxy (MOVPE). The growth temperature of the *n*-type GaN was 1025 °C. GaN layer thicknesses and carrier concentrations at room temperature were in ranges of

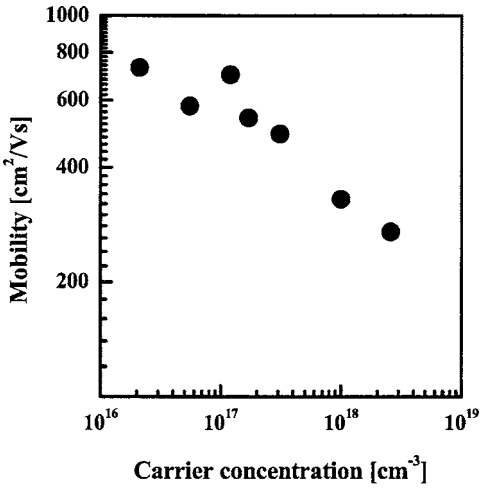

FIG. 1. Room-temperature electrical properties of *n*-type GaN layers used for photoelectrochemical evaluations. The Hall mobility and carrier concentration were measured by the van der Pauw method.

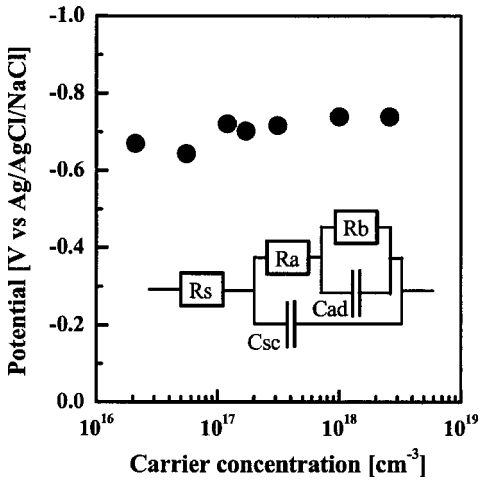

FIG. 2. Flatband potentials of *n*-type GaN layers with various carrier concentrations. The electrolyte was 1.0 mol/l HCl. The potentials were obtained by the Mott-Schottky plot. The frequency range for the Mott-Schottky plot was from 50 to 20 000 Hz in order to eliminate the effect of slow carrier transfer process. The amplitude was 20 mV. The reference electrode was Ag/AgCl/NaCl. The equivalent circuit for impedance analysis is also indicated. The capacitance used for flatband calculation was C_{sc} in the equivalent circuit.

2.8–6.2 μm and $n=2\times10^{16}-3\times10^{18}$ cm^{-3}, respectively. The thickness was measured by using secondary electron microscope. The electrical properties were determined by using Hall measurements (the van der Pauw method). The crystal quality was evaluated by full width at half maximum (FWHM) of x-ray rocking curve (ω scan) for (0002) reflection of GaN layer.

Ti(10 nm)/Au(50 nm) depositions were made on the periphery of the samples and alloyed in order to make Ohmic contacts. The contact area with an electrolyte was 10 mm in diameter and was photoilluminated using 150 W Xe lamp. A reference electrode was Ag/AgCl/NaCl [sodium-chloride-saturated silver-chloride electrode (SSSE)]. Its electrode potential is $E(\mathrm{AgCl/Ag})=+0.212$ V versus normal hydrogen electrode. The reference electrode was not used at static photocurrent density measurements and the experiment for H_2 gas generation. A counter electrode was made of Pt. The electrolyte was selected to be 1.0 mol/l HCl (pH=0.2) in order to minimize the effect of photoanodic dissolution.[8,9] A potentiostat (Solartron SI-1280B) and a gas chromatograph (Shimadzu GC-9A) were used to evaluate the electrochemical properties and gas composition, respectively.

III. RESULTS AND DISCUSSION

A. Flatband potentials of *n*-type GaN

Carrier concentration and mobility, measured by the van der Pauw method of the *n*-type GaN, used for photoelectrochemical evaluation are shown in Fig. 1. Since *n*-type GaN was used, the measured carriers in Fig. 1 were electrons. FWHM's of x-ray rocking curve for (0002) reflection from these samples were almost the same, and were in the range between 200 and 300 arc sec. From the relationship between carrier concentration and mobility and from the FWHM's of x-ray rocking curve, the crystallinity of *n*-type GaN used here was fairly good and almost identical.

Flatband potentials obtained from the Mott-Schottly plot are shown in Fig. 2. The capacitance for the plot was calculated from impedance fitting using an equivalent circuit.[5] The frequency range for the impedance measurement for each applied potential was from 50 to 20 000 Hz. The equivalent circuit for impedance fitting is also shown in the inset of Fig. 2. R_s in the equivalent circuit denotes a series resistor of an electrolyte and a semiconductor. C_{sc} is the capacitance for a semiconductor/electrolyte interface. The others indicate the Faraday impedance for a semiconductor/electrolyte interface. That is, the symbol R_a denotes the resistor in the space charge region, C_{ad} is the capacitor caused by the intermediate states like recombination center near the semiconductor/electrolyte interface, and R_b is the resistor at the region with the intermediate states. We neglected the slow diffusion component (<1 Hz) or the Warburg impedance because the measured frequency was relatively of higher range.[10] Since C_{sc} was the space charge capacitance for a semiconductor/electrolyte circuit, this C_{sc} was used for the C of the Mott-Schottky plot. Flatband potentials of the samples exhibited almost the same value around −0.7 V vs SSSE. This indicates that the flatband potential of *n*-type GaN is independent of carrier concentration. The same relationship observed other semiconductors, explained as the pinning of flatband potential.[1]

B. Current density versus bias characteristics

The relationships between the static photocurrent density and bias are shown in Fig. 3. We applied static bias (V_{CE}) to the *n*-type GaN working photoelectrodes versus the Pt counterelectrode. The current density was defined as current divided by the aqueous contact area of the *n*-type GaN working electrode. We also defined the start point of V_{CE} as onset voltage, where current density increased abruptly. The onset voltages were almost the same values ($V_{CE}=-0.2$ V). The current densities were saturated at around $V_{CE}=+1.0$ V for all samples. To find the optimized carrier concentration for the photocurrent at zero bias, we plotted the photocurrent

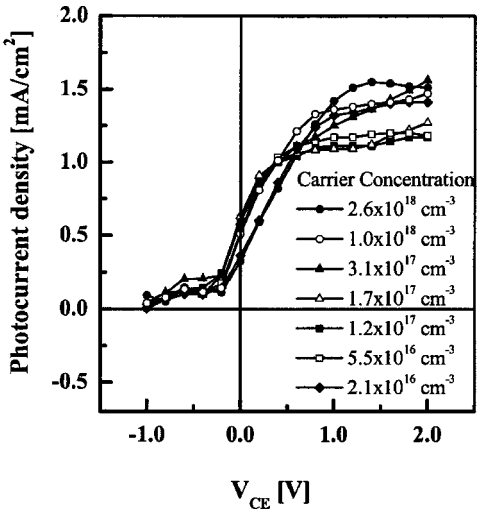

FIG. 3. Relationships between static photocurrent density and applied bias to *n*-type GaN working electrode vs Pt counterelectrode (V_{CE}). The electrolyte was 1.0 mol/l HCl.

densities at zero bias versus carrier concentration as shown as closed circles in Fig. 4. It was found clearly that the photocurrent density became the maximum value at the carrier concentration of around 1.7×10^{17} cm^{-3}.

We checked several times the relationships where the samples obtained are not only from different series of MOVPE growth but also from different kinds of electrode deposition, which are also shown as open circles in Fig. 4. The FWHM's of x-ray rocking curve of (0002) for the repeat samples were less than 450 arc sec. As far as the relationships between carrier concentration and mobility and the FWHM range of x-ray rocking curve of (0002) reflection are satisfied as discussed in Sec. III A, similar photocurrent dependent on carrier concentration was observed in our experimental setup.

The photocurrents in the saturated plateau at high anodic bias region had relatively large discrepancies as shown in Fig. 3. The reason is discussed at the end of Sec. III D. The origin of the current before the onset voltage was probably some reactions with easy-oxidized ingredients in the electrolyte.

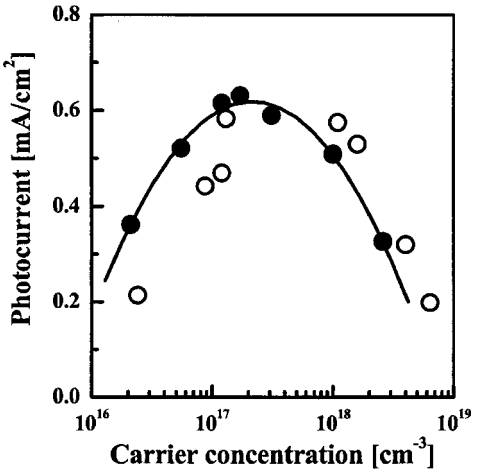

FIG. 4. The dependence of the photocurrent density on the carrier concentration at V_{CE}=0.0 V. Closed circles show the data taken from the samples shown in Fig. 3. Open circles are the reference data taken from the different condition of growth and electrode deposition to check the carrier concentration dependence repeatability. The electrolyte was 1.0 mol/l HCl. The solid line is a guide to the eye.

C. Charge transfer process at the semiconductor/electrolyte interface

Understanding the response of semiconductor/electrolyte interface by illumination is very important to explain the photocurrent dependent on carrier concentration of semiconductor. Electrolyte behaves like metal conductor if it has a lot of ions. In this case, the model for the interface between semiconductor and transparent metal proposed by Gartner is presumably valid for that between semiconductor and electrolyte in general.[11] However, the Gartner model requires three hypotheses when we assume a *n*-type semiconductor.

(1) The electron flow between semiconductor and electrolyte does not occur, because the band bending of space charge region is sufficiently large.
(2) The recombination rate in the semiconductor space charge region is zero, because the drift speed of carriers in the space charge region is fast.
(3) The hole concentration at the edge of space charge region is zero.

Precise model under quasiequilibrium condition including electron transfer and recombination was proposed by Reichman.[12] Thus, we used the Reichman model in order to explain the relationship between the photocurrent density at zero bias and the carrier concentration of *n*-type GaN.

In the Reichman model, the current density J across a semiconductor/electrolyte interface is described as

$$J_n = -I_n^0\left(\frac{n_s - n_{s0}}{n_{s0}}\right) = -I_n^0\left(\frac{n_s}{n_{s0}} - 1\right), \tag{1}$$

$$J_p = I_p^0\left(\frac{p_s - p_{s0}}{p_{s0}}\right) = I_p^0\left(\frac{p_s}{p_{s0}} - 1\right), \tag{2}$$

$$J = J_n + J_p, \tag{3}$$

where J_x is the electron/hole current density, I_{x0} is the electron/hole exchange current parameter, x_s is the electron/hole interface concentration, and x_{s0} is the electron/hole equilibrium interface concentration [here, $x=n$(electron)/p(hole)].

The semiconductor in the model can be divided into two regions, that is, one is a space charge region where the conduction and valence bands are bending near the semiconductor/electrolyte interface, and the other is a neutral region which is deeper than the space charge region and no electric field exist. The diffusion equation for minority carrier in the neutral region is

$$D\frac{\partial^2 p}{\partial x^2} - \frac{p - p_0}{\tau} + I_0\alpha\exp(-\alpha x) = 0, \tag{4}$$

where D is the diffusion coefficient, p is the hole concentration, p_0 is the equilibrium hole concentration, τ is the lifetime of the minority carrier, I_0 is the monochromatic phonon

flux incident on the semiconductor, and α is the absorption coefficient. The hole current density at the edge of space charge region J_w is obtained by using the solution of Eq. (4) with the boundary condition of $p=p_0$ at $x=\infty$ and $p=p_w$ at $x=W$ (W is the edge of the space charge region.),

$$J_w = -J_0\left(\frac{p_w}{p_0} - 1\right) + \frac{qI_0\alpha L \exp(-\alpha W)}{1+\alpha L}, \tag{5}$$

$$J_0 = \frac{qp_0 L}{\tau^2}, \tag{6}$$

where q is the elementary charge and L is the hole diffusion length. The values of p_0, L, and W are also given by

$$p_0 = \frac{n_t^2}{N}, \tag{7}$$

$$L = (D\tau)^{0.5}, \tag{8}$$

$$W = \left\{\frac{2\varepsilon_0\varepsilon_r}{eN_D}(V - V_{\mathrm{fb}})\right\}^{1/2}, \tag{9}$$

where n_i is the intrinsic carrier density, N is the carrier concentration (n type), V is the voltage applied to the semiconductor, V_{fb} is the flatband potential, N_D is the donor concentration, ε_r is a dielectric constant, and ε_0 is the perimittivity of vacuum.

On the other hand, the current density in the space charge region generated by photon absorption J_{SCR}^G is

$$J_{\mathrm{SCR}}^G = qI_0(1 - \exp(-\alpha W)). \tag{10}$$

The hole current density transferred across the semiconductor/electrolyte interface without recombination in the space charge region is given by the summation of Eqs. (5) and (10),

$$J_p = J_w + J_{\mathrm{SCR}}^G, \tag{11}$$

$$J_p = -J_0\left(\frac{p_w}{p_0} - 1\right) + \frac{qI_0}{1+\alpha L}[1 + \alpha L - \exp(-\alpha W)]. \tag{12}$$

Since the Gartner model regards $p_w=0$, the hole current density of the Gartner model J_g is obtained from Eq. (11),

$$J_g = J_0 + \frac{qI_0}{1+\alpha L}[1 + \alpha L - \exp(-\alpha W)]. \tag{13}$$

The Reichman model assumes quasiequilibrium conditions of electron and hole concentrations in the space charge region,

$$n_s = n_w\gamma_1 \exp\left(-\frac{q(V - V_{\mathrm{fb}})}{kT}\right), \tag{14}$$

$$p_s = p_w\gamma_2 \exp\left(\frac{q(V - V_{\mathrm{fb}})}{kT}\right), \tag{15}$$

where n_w is the electron concentration at the edge of the space charge region, k is the Boltzmann constant, T is the absolute temperature, and γ_1 and γ_2 are constants. When one considers equilibrium condition of $V=0$, $n_w=n_0$, $n_s=n_{s0}$, $p_w=p_0$, and $p_s=p_{s0}$ are satisfied. Thus, n_0 and p_0 under equilibrium condition are calculated by using Eqs. (14) and (15)

Inserting Eq. (15) with its equilibrium condition into Eq. (2), p_w/p_0 is obtained without γ_2. One obtains J_p using Eq. (13) into Eq. (12) with this p_w/p_0,

$$J_p = \frac{J_g - J_0\exp(-qV/kT)}{1 + (J_p/I_p^0)\exp(-qV/kT)}. \tag{16}$$

For majority carrier in n-type semiconductor, $n_w \approx n_0$ is achieved because the carrier generated by photon absorption is much smaller than free carrier. Thus, one obtains J_n by inserting n_w/n_0, obtained from the equilibrium condition of Eq. (14), into Eq. (1),

$$J_n = -I_n^0\left[\exp\left(-\frac{qV}{kT}\right) - 1\right]. \tag{17}$$

The total current density transferred across the semiconductor/electrolyte interface without carrier recombination in the space charge region is obtained from Eq. (3) using Eqs. (16) and (17).

The effect of recombination in the space charge region is described using the model of Sah *et al.*[12,13] The recombination current density in the space charge region is

$$J_{\mathrm{SCR}}^R = K\left(\frac{p_s}{p_{s0}}\right)^{0.5}, \tag{18}$$

$$K = \frac{\pi kTn_i W \exp(-qV/2kT)}{4\tau(V - V_{\mathrm{fb}})}. \tag{19}$$

The hole current density transferred across the semiconductor/electrolyte interface with recombination in the space charge region is instead of the case without recombination Eq. (11),

$$J_p = J_w + J_{\mathrm{SCR}}^G - J_{\mathrm{SCR}}^R. \tag{20}$$

Inserting Eqs. (5), (10), (13), and (18) into Eq. (20), J_p is given by

$$J_p = -J_0\frac{p_w}{p_0} + J_g - K\left(\frac{p_s}{p_{s0}}\right)^{0.5}. \tag{21}$$

Using Eqs. (2) and (15) and its equilibrium condition, p_s/p_{s0} in Eq. (21) is solved.

The hole current density transferred across the semiconductor/electrolyte interface with recombination in the space charge region is inserting the p_s/p_{s0} into Eq. (2) instead of the case without recombination in Eq. (16),

$$J_p = I_p^0\left\{\left[\frac{-K + (K^2 + 4AB)^{0.5}}{2A}\right]^2 - 1\right\}, \tag{22}$$

with the additional abbreviations,

$$A = I_p^0 + J_0\exp\left(-\frac{qV}{kT}\right), \tag{23}$$

$$B = I_p^0 + J_g. \tag{24}$$

The total current density transferred across the semiconductor/electrolyte interface with carrier recombina-

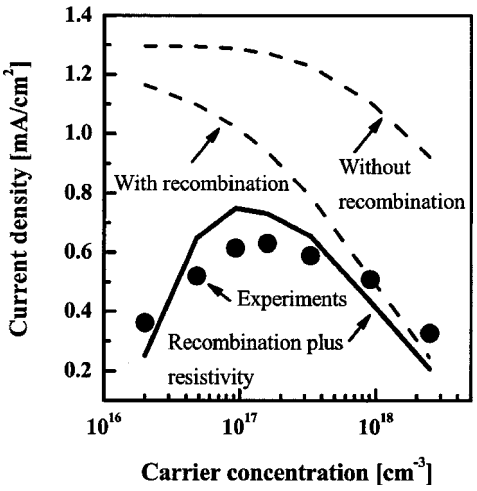

FIG. 5. Relationships between calculated photocurrent densities and carrier concentration of the *n*-type GaN photoelectrodes. The experimental data of the photocurrent densities are also plotted as closed circle. The broken line shows the calculated photocurrent from the Reichman model with and without recombination in the space charge region. The solid line shows the calculated photocurrent which takes into account of the system resistances and the recombination.

tion in the space charge region is obtained from Eq. (3) using Eqs. (17) and (22).

D. Photocurrent density dependent on carrier concentration

The minority carrier diffusion length L used the expression of

$$L = \sqrt{\frac{kT}{e}\mu(n)\tau}, \tag{25}$$

where $\mu(n)$ is the hole carrier mobility in *n*-type semiconductor. The dependence of the hole (majority carrier) mobility on carrier concentration, determined for *p*-type GaN, was used for $\mu(n)$.[14] The minority carrier diffusion coefficient D was calculated using Eqs. (8) and (25). The lifetime of the minority carrier τ is proposed as

$$\tau = \frac{1}{BN}, \tag{26}$$

where B is the radiative constant as 1.1×10^{8} cm^3/s.[15] The absorption coefficient α was reported around 1.0×10^{5} cm^{-1} just over the band-gap energy, and getting higher with increasing photon energy.[15] Therefore, we used $\alpha=3.0\times10^{5}$ cm^{-1} because continuous Xe lamp was illuminated to the sample for our experiments. The hole and electron exchange parameters of GaN were difficult to find for the calculations. Thus, we used the values which Reichman proposed, that is, $I_p^0=1.0\times10^{-5}$ mA/cm^2 and $I_n^0=1.0\times10^{-5}$ mA/cm^2.[12] The incident photon flux I_0 was selected as 8.13×10^{18} photons/cm^3, where the maximum photocurrent was 1.3 mA/cm^2.

The results of calculated total photocurrent density at zero bias with and without recombination in the space charge region are shown in Fig. 5. The photocurrent density without recombination was calculated using Eqs. (3), (16), and (17).

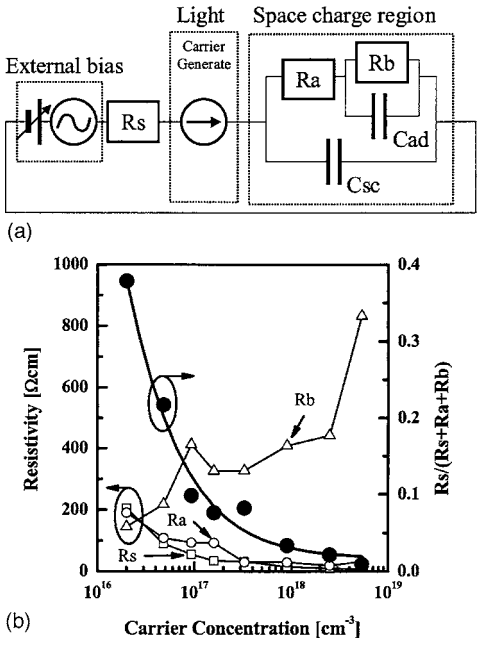

FIG. 6. (a) The current circuit model for the photoelectrochemical system. (b) The dependence of the series and parallel resistances on carrier concentration of the *n*-type GaN photoelectrode/electrolyte system obtained from the impedance measurements under illumination. The frequency range for the electric circuit evaluation was from 100 to 20 000 Hz, and the amplitude was 20 mV. The applied voltage was −0.2 V vs Ag/AgCl/NaCl. The ratio of series resistance and the total resistance of the system as a function of carrier concentration is also plotted.

The photocurrent density with recombination was calculated using Eqs. (3), (17), and (22). Both calculated lines are monotonously decreasing with increasing carrier concentration. The calculated current density line without recombination has large discrepancy with the experimental results. On the other hand, the calculated current density line with recombination shows agreement with the experimental values of photocurrent density at the higher carrier concentrations, but does not fit in the lower carrier concentration region. These results show that the recombination in space charge region plays an important role for the determination of photocurrent density in the higher carrier concentration region.

It is clear that we need to consider some effect to decrease the photocurrent in the lower carrier concentration region. The photoelectromotive force is mainly defined by the band bending of semiconductor in space charge region and the light intensity at zero bias. Thus, the current of the circuit was probably estimated using the total resistance of the whole electrochemical system. The distance of the current path from the photoilluminated area of GaN to the metal contact on the surface was several millimeters for our experiments. The thickness of the current path was a few micrometers because we used insulating sapphire as a substrate. Thus, the resistance of the thin current path would be very high, especially in the case of the lower carrier concentrations. To confirm the effect of resistance, we evaluated the resistance calculated from the impedance measurements under illumination. The equivalent circuit for the system used the resistance calculation as shown in Fig. 6(a). The resistances (R_s, R_a, and R_b) and the ratio of $R_s/(R_s+R_a+R_b)$ versus carrier concentration are shown in Fig. 6(b). The photocurrents were

measured at V_{CE}=0.0 V. Thus, the resistance was measured at the bias of −0.2 V SSSE, because the points of the strong increase in the photocurrent measured were −0.4 V vs SSSE, where the points were V_{CE}=−0.2 V. The series resistance R_s decreased with increasing carrier concentration. It should be pointed out that the sum of R_a and R_b increased with increasing carrier concentration.

The bias of the space charge region V_{int} is calculated considering the voltage drop at the external resistance R_s,

$$V_{int} = V_{fb} + (V - V_{fb})\left(1 - \frac{R_s}{R_s + R_a + R_c}\right), \quad (27)$$

where V is the external applied bias. The photocurrent density at zero bias with recombination in the space charge region [Eqs. (3), (17), and (22)] and using V_{int} of Eq. (27) instead of applied bias V (here, V=0.0 V) is also shown in Fig. 5. V_{fb}=−0.7 V was used for the calculation. The shape of the calculated current density line is similar to that of the photocurrent densities from the experiments. Thus, we concluded that the photocurrent efficiency was explained by the Reichman model with the recombination in space charge region and by the resistance of the photoelectrochemical system. The shapes of the measured and the estimated photocurrent densities have still some difference. This difference would be originated from the decrease of absorption coefficient α with conductivity in the lower carrier concentration region, the shorter minority carrier diffusion length L with increasing carrier concentration, the carrier recombination model, and the mixing effect of the materials in the electrolyte.

This model roughly explains the reason why the saturated photocurrent region at high anodic bias had relatively large discrepancies. Under high anodic bias, the carriers are accelerated by the electric field generated by the bias. Therefore, the depths of light absorption and space charge region are not much influenced to carrier transfer, and only fast carrier recombination is probably dominant for carrier loss. In Fig. 3, relatively low carrier concentration samples show the lower photocurrent densities under high anodic bias condition except for the sample with the carrier concentration of 2.1×10^{16} cm^{-3}. This probably indicates that the resistivity of the whole system influences the carrier loss under high anodic bias condition. For the case of the carrier concentration of 2.1×10^{16} cm^{-3}, carrier recombination via doping impurities would also affect the carrier loss because the sample is an undoped one. Further investigations are required to know the detail of the discrepancies of the saturated photocurrent.

E. H_2 generation at zero bias

The photocurrent density at the zero bias became the maximum value at the carrier concentration of 1.7×10^{17} cm^{-3}, as shown in Fig. 4. Thus, we studied the gas generation using n-type GaN with the carrier concentration of 1.7×10^{17} cm^{-3} by photoelectrolysis without bias, that is, V_{CE}=0.0 V. A bias was required to generate H_2 gas from a counterelectrode for GaN with a carrier concentration of 1.8×10^{18} cm^{-3} as we reported.[9] Since the H_2 gas generation is from a counterelectrode, the gas observation depends on the photocurrent. We need a photocurrent at least approximately 0.4 mA to observe H_2 gas generation clearly by eyes at the beginning in our experience. This dependence is not clearly explained until now, but some residuals in solution would cause to prevent clear H_2 generation. Thus, H_2 generation were observed if we would wait long time at the case of the carrier concentration of 1.8×10^{18} cm^{-3}. The photocurrent density at zero bias for the previous case was around 0.4 mA/cm^2, and was 2/3 of the optimized case. The illuminated area of our experimental setup was 0.785 cm^2, thus, the previous photocurrent was 0.31 mA. This is probably why we have not observed H_2 gas generation for GaN with a carrier concentration of 1.8×10^{18} cm^{-3} under zero bias condition at the beginning. Since the photocurrent of carrier concentration optimized was 0.47 mA at zero bias, we expected to observe H_2 gas generation from a counterelectrode clearly from the beginning.

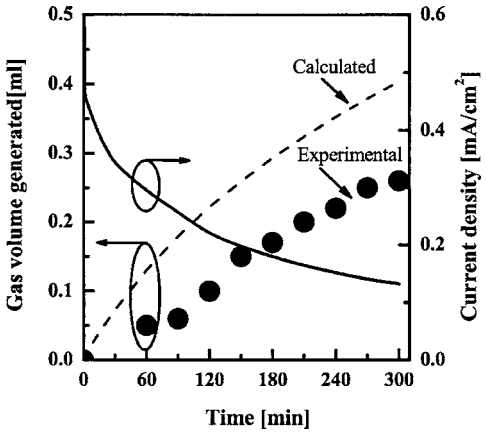

FIG. 7. Time dependences of gas volume generated at Pt counterelectrode and photocurrent density. The n-type GaN working photoelectrode was under illumination and in aqueous 1.0 mol/l HCl. The bias between the illuminated GaN working electrode and the Pt counterelectrode was not applied (V_{CE}=0.0 V). The H_2 gas volume calculated from photocurrent is also plotted as broken line.

The time dependences of the gas generation from the Pt counterelectrode and of the current density are shown in Fig. 7. As can be seen, we have achieved gas generation at zero bias. The composition of the gas generated at the Pt counterelectrode in 1.0 mol/l HCl after 300 min was 80% H_2, 19% N_2, and 1% O_2. The existence of hydrogen indicates that the reduction of water occurs at the counterelectrode. The amount of the gas generation was, however, approximately 1/3 compared to that of the bias applied V_{CE}=1.0 V.[9] The amount was also smaller than the expected H_2 gas generation calculated from the current, which is also plotted in the graph. The discrepancy between the calculated and experimental H_2 gas generation is relatively large, probably because of the dissolution of H_2 gas into electrolyte and occurrence of some other reduction.

Etching of the n-type GaN working electrode after 300 min illumination was almost zero within the weight measurement error (less than 0.2 μm in thickness). This means that the reaction at the surface of the n-type GaN working electrode was not GaN decomposition but Cl^- oxidation as expected.[8] The surfaces after photoelectrochemical

reaction in HCl were, however, changes to rough by observed scanning electron microscope. In addition, the oxygen concentration at the GaN surface after the reaction was increased compared with as-grown GaN surface even in HCl solution by using energy-dispersive x-ray spectroscopy. This surface oxide would prevent the current flow, and cause the decrease of the photocurrent in time.

We calculated the conversion efficiency from light to chemical energy. The total conversion efficiency is defined as

$$\eta_{\text{eff}} = \frac{(E_{\text{rev}}^0 - V_{\text{CE}})j_p}{P_0} \times 100, \tag{28}$$

where $\eta_{\text{eff}}(\%)$ is the energy conversion efficiency, E_{rev}^0 (V) is the voltage for the electrode voltage difference from the hydrogen generation and oxidation, V_{CE} (V) is the applied voltage between a photoworking electrode and a counterelectrode, j_p (mA/cm^2) is the photocurrent density, and P_0 (W/cm^2) is the power density of light.[16] When we used $E_{\text{rev}}^0 = 1.40$ V for Cl^- reduction instead of water splitting because of the HCl electrolyte, $j_p = 0.48$ mA/cm^2 at 1 min after the illumination and $P_0 = 110$ mW/cm^2, the η_{eff} was obtained to be 0.61%. This is the first time to succeed to achieve H_2 gas generation without bias ($V_{\text{CE}} = 0.0$ V) using *n*-type GaN in 1.0 mol/l HCl solution.

IV. CONCLUSION

The dependence of photoelectrochemical properties on carrier concentration of *n*-type GaN in 1.0 mol/l HCl (pH = 0.2) was investigated. The flatband potential was not changed in carrier concentration. The shapes of static current density versus bias curves were also similar to each other, however, the photocurrent density at zero bias ($V_{\text{CE}} = 0.0$ V) depended on the carrier concentration. The sample with the carrier concentration of 1.7×10^{17} cm^{-3} revealed the maximum photocurrent without bias. The photocurrent dependent on the carrier concentration was explained by the charge transfer model at semiconductor/electrolyte interface with the recombination in space charge region and the resistance of the photoelectrochemical system. H_2 gas generation at a Pt counterelectrode without bias was observed at the carrier concentration having the maximum photocurrent.

ACKNOWLEDGMENTS

The authors would like to thank Dr. Kazuhide Kusakabe for helpful discussions. The authors also thank Kuniyoshi Okamoto for technical assistance.

[1] A. J. Nozik and R. Memming, J. Phys. Chem. **100**, 13061 (1996).
[2] M. Tomkiewicz and H. Fay, Appl. Phys. **18**, 1 (1979).
[3] S. S. Kocha, M. W. Peterson, D. J. Arent, J. M. Redwing, M. A. Tischler, and J. A. Turner, J. Electrochem. Soc. **142**, L238 (1995).
[4] I. M. Huygens, K. Strubbe, and W. P. Gomes, J. Electrochem. Soc. **147**, 1797 (2000).
[5] K. Fujii, T. Karasawa, and K. Ohkawa, Jpn. J. Appl. Phys., Part 2 **44**, L543 (2005).
[6] K. Fujii and K. Ohkawa, Jpn. J. Appl. Phys., Part 2 **44**, L909 (2005).
[7] K. Fujii, K. Kusakabe, and K. Ohkawa, Jpn. J. Appl. Phys., Part 1 **44**, 7433 (2005).
[8] I. M. Huygens, A. Theuwis, W. P. Gomes, and K. Strubbe, Phys. Chem. Chem. Phys. **4**, 2301 (2002).
[9] K. Fujii and K. Ohkawa, J. Electrochem. Soc. **153**, A468 (2006).
[10] A. Meier, D. C. Selmarten, K. Siemoneit, B. B. Smith, and A. J. Nozik, J. Phys. Chem. B **103**, 2122 (1999).
[11] W. W. Gartner, Phys. Rev. **116**, 84 (1959).
[12] J. Reichman, Appl. Phys. Lett. **36**, 574 (1980).
[13] C. T. Sah, R. N. Noyce, and W. Shockley, Proc. IRE **45**, 1228 (1957).
[14] L. Chemyak, A. Osinsky, H. Temkin, J. W. Yang, Q. Chen, and M. Asif Khan, Appl. Phys. Lett. **69**, 2531 (1996).
[15] J. F. Muth, J. H. Lee, I. K. Shmagin, R. M. Kolbas, H. C. Casey, Jr., B. P. Keller, U. K. Mishra, and S. P. DenBaars, Appl. Phys. Lett. **71**, 2572 (1997).
[16] S. U. M. Khan, M. Al-Shahry, and W. B. Ingler, Jr., Science **297**, 2243 (2002).